Appl. Chem. Eng., Vol. 26, No. 6, December 2015, 746-752
http://dx.doi.org/10.14478/ace.2015.1112

Communication

염화제일수은과 일산화질소의 물리적 승화법 공정에서의 확산-대류에 미치는 에스펙트 비율의 영향

김극태

한남대학교 화공신소재공학과
(2015년 10월 14일 접수, 2015년 11월 4일 심사, 2015년 11월 10일 채택)

Effects of Aspect Ratio on Diffusive-Convection During Physical Vapor Transport of Hg_2Cl_2 with Impurity of NO

Geug-Tae Kim

Department of Advanced Materials and Chemical Engineering, Hannam University, 1646, Yuseong-daero, Yuseong-gu, Daejeon, 34054 Rep. of KOREA
(Received October 14, 2015; Revised November 4, 2015; Accepted November 10, 2015)

초 록

본 연구에서는 Hg_2Cl_2-NO의 물리적 승화법 공정에서의 확산-대류에 미치는 에스펙트 비율(길이/폭)의 영향에 대한 것이다. 원료물질 영역과 결정영역에서의 온도 차 20 K, 벽에서의 선형 온도분포를 가진 계에서, 대류의 영향 때문에, 총몰플럭스와 상호계면에서의 비균일성에 관하여서는, 에스펙트 비율이 2인 경우가 비율이 5인 경우보다 상당히 크다. 지상중력 하에서의 최고 총몰플럭스는 지상중력의 0.1 상태에 비하여 대략 2배 정도 크다. 에스펙트 비율을 2에서 5로 증가시켰을 때, 확산-대류형이 대류형으로 전이되며, 또한 확산의 강도도 확산-대류형의 강도를 지배하게 된다.

Abstract

This study investigates the effects of aspect ratio (transport length-to-width) on diffusive-convection for physical vapor transport processes of Hg_2Cl_2-NO system. For a system with the temperature difference of 20 K between an interface at the source material region and growing crystal interface, the linear temperature profiles at walls, the total molar fluxes at Ar = 2 are much greater than Ar = 5 as well as the corresponding nonuniformities in interfacial distributions due to the effect of convection. The maximum total molar flux at the gravitational acceleration of 1 g_0 is greater twice than at the level of 0.1 g_0, where g0 denotes the gravitational acceleration on earth. With increasing aspect ratio from 2 to 5, a diffusive-convection mode is transited into the diffusion mode, and then the strength of diffusion is predominant over the strength of diffusive-convection.

Keywords: *aspect ratio, physical vapor transport*

1. Introduction

Mercurous chloride (Hg_2Cl_2) single crystals have applications for acousto-optic and opto-electronic devices such as Bragg cells, X-ray detectors operating at ambient temperatures[1]. The equimolar Hg_2Cl_2 compound decomposes to two liquids at a temperature near 525 ℃ where the vapor pressure is above 20 atm[2,3]. Because of its high vapor pressure and decomposition, Hg_2Cl_2 cannot be solidified as a single crystal directly from the stoichiometric melt and are currently produced using the physical vapor transport (PVT) technology. In recent years, many authors have conducted studies on the widespread commercialization of SiC[4-9], AlN[10], ZnTe[11], $Cd_{0.9}Zn_{0.1}Te$[12] by the PVT method, also referred to as a mechanism of sublimation-condensation: the source component-bearing species are vaporized from the source material and recrystallized on a seed crystal, in closed silica glass ampoules in temperature gradient imposed between the source material and the growing crystal. Cai et al.[13] discussed on the enhanced synthesis of Sn nanowires with aid Se atoms via physical vapor transport. By the vapor transport techniques, the fabrications of thin solid films of polydiacetylene, CdTe, Alq_3 were reported[14-16]. Choubey et al.[17] used the multi-tube physical vapor transport (PVT) method to prepare (Cd, Zn) Te crystals and to perform characterization experiments of X-ray diffraction (XRD), infra-red (IR) mapping, photoluminescence (PL) as well as measurements of mobility lifetime and current-voltage. Shi et al.[18] investigated the mechanism of nucleation and the growth of SiC whiskers, and prepared 6H-type SiC whiskers.

Author: Hannam University,
Department of Advanced Materials and Chemical Engineering, 1646, Yuseong-daero, Yuseong-gu, Daejeon, 34054 Rep. of KOREA
Tel: +82-42-629-8837 e-mail: geugtaekim@gmail.com

pISSN: 1225-0112 eISSN: 2288-4505

Zotov et al.[19] made dense La-Sr-Fe-Co oxygen transport membranes in applications for metal supports deposited by low plasma spraying physical vapor deposition. Fanton et al.[20] discussed over the effects of hydrogen on the properties of SiC crystals grown by the PVT from a viewpoint of thermodynamic considerations and experimental results. They showed the level of boron contamination in all samples was not affected by the addition of hydrogen. Su et al.[21] used the self-seeded PVT method in horizontal orientations to prepare ZnSe crystals and studied on the effects of convection which occurs in the vapor phase. Paorici et al.[22] have performed the experiments of PVT techniques for urotropine to prove one-dimensional diffusion model to get qualitative results: low mass transport rates of polycrystalline urotropine imply high amounts of volatile impurities.

Over the past 30 years many theoretical modeling studies on transport phenomena in PVT have been extensively investigated by Rosenberger's research team, whose typical papers are found in refs.[23-24]. Using the finite element method, Tebbe et al.[25] extended for transition to chaos flow fields in specialty materials of mercurous chloride in applications of microgravity experiments. They have addressed the underlying phenomena in the PVT processes on the relative importance and influencing parameters of diffusion-advection, thermal and/or solutal convection on mass transport. More recently, Alsaady et al.[26] reported the thermo-magnetic convective effects of ferrofluid, and Qin et al.[27] discussed over buoyancy-thermocapillary convection of volatile fluids under their vapors from a viewpoint of heat and mass transfer. In one's earlier paper, a mixture of Hg_2Br_2 and Br_2 was considered. In this paper, one investigates the effects of aspect ratio on diffusive thermally buoyancy-driven convection during the PVT processes of Hg_2Cl_2 crystal growth with a mixture of Hg_2Cl_2 vapor and impurity of Nitric Oxide (NO). For this numerical analysis of the PVT processes, a two-dimensional model is chosen in horizontally oriented, cylindrical, closed ampoules in a two-zone furnace system.

2. Model Description

A model was created with appropriate geometry, boundary conditions, and material properties of mercurous chloride. As shown in Figure 1, the geometry is a two-dimensional rectangular enclosure with aspect ratio (transport length L-to- height H) of 2 and of 5. The source is maintained at a temperature T_s, while the growing crystal is at a temperature T_c, with $T_s > T_c$. PVT of the transported component A (Hg_2Cl_2) occurs inevitably, due to presence of impurities, with the presence of a component B (NO). Thermo-physical properties of the vapor mixture of A (Hg_2Cl_2) and component B (NO) are assumed to be constant, except for the density. The density is assumed constant except the buoyancy body force term, which would be a function of both temperature and concentration. The interfaces are assumed to be flat for simplicity and the finite normal velocities at the interfaces can be expressed by Stefan flow deduced from the one-dimensional diffusion-limited model[28], which would provide the coupling between the fluid dynamics and species calculations. The tangential component of the mass average velocity of the vapor at the interfaces vanishes. Thermodynamic equilibria are assumed at the interfaces so that the

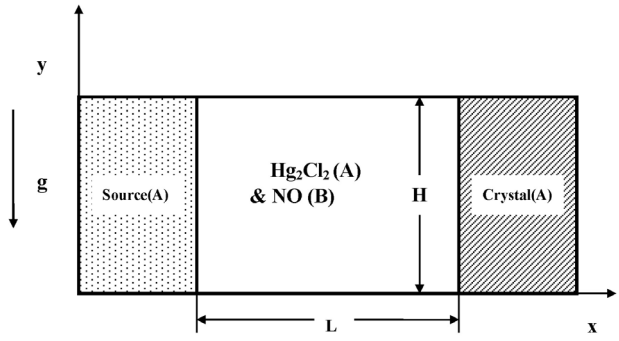

Figure 1. Schematic description of a two-dimensional PVT model for a Hg_2Cl_2-NO system.

mass fractions at the interfaces are kept constant at $\omega_{A,s}$ and $\omega_{A,c}$. On the vertical non-reacting walls appropriate velocity boundary conditions are no-slip, the normal concentration gradients are zero, and wall temperatures are imposed as a linear temperature gradients. The transport of fluid within a rectangular PVT crystal growth reactor is governed by a system of elliptic, coupled conservation equations for mass (continuity), momentum, energy and species (diffusion) can be represented by the generic Eq. (1)[29] with their appropriate boundary conditions Eqs. (2) through (4). Let u_x, u_y denote the velocity components along the x- and y-coordinates in the x, y rectangular coordinate, and let T, ω_A, p denote the temperature, mass fraction of species A (Hg_2Cl_2) and pressure, respectively, where the superscript of * denotes the dimensionless[29].

$$\nabla \bullet (\rho u \phi) = \nabla \bullet (\Gamma \nabla \phi) + S, \tag{1}$$

On the walls ($0 < x^* < L/H$, $y^* = 0$ and 1):

$$\begin{aligned} &u^*(x^*,0) = u^*(x^*,1) = v^*(x^*0) = v^*(x^*,1) = 0 \\ &\frac{\partial \omega_A^*(x^*,0)}{\partial y^*} = \frac{\partial \omega_A^*(x^*,1)}{\partial y^*} = 0, \\ &T^*(x^*,0) = T^*(x^*,1) = \frac{T - T_c}{T_s - T_c} \end{aligned} \tag{2}$$

On the source ($x^* = 0$, $0 < y^* < 1$):

$$\begin{aligned} u^*(0,y^*) &= -\frac{1}{Le}\frac{\Delta\omega}{(1-\omega_{A,s})}\frac{\partial \omega_A^*(0,y^*)}{\partial x^*}, \\ v^*(0,y^*) &= 0, \\ T^*(0,y^*) &= 1, \\ \omega_A^*(0,y^*) &= 1. \end{aligned} \tag{3}$$

On the crystal ($x^* = L/H$, $0 < y^* < 1$):

$$\begin{aligned} u^*(L/H,y^*) &= -\frac{1}{Le}\frac{\Delta\omega}{(1-\omega_{A,c})}\frac{\partial \omega_A^*(L/H,y^*)}{\partial x^*} \\ v^*(L/H,y^*) &= 0, \\ T^*(L/H,y^*) &= 0, \\ \omega_A^*(L/H,y^*) &= 0. \end{aligned} \tag{4}$$

Table 1. Typical Thermo-physical Properties Used in this Study (M_A = 472.086, M_B = 30.01)

Transport length, L	10 cm
Height, H	2 cm
Source temperature, T_s	613.15 K
Crystal temperature, T_c	593.15 K
Thermal diffusivity	0.05 cm^2/s
Kinematic viscosity, μ	0.12 cm^2/s
Diffusivity, D_{AB}	0.64 cm^2/s
Thermal expansion coefficient, β	0.0016 K^{-1}
Concentration number, Cv	1.07
Total system pressure, P_T	293.54

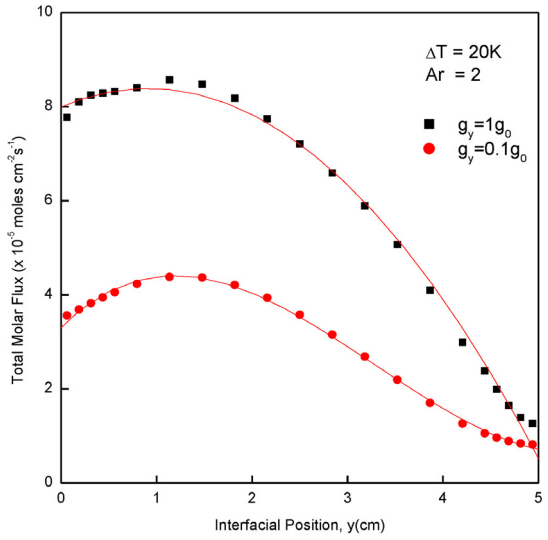

Figure 2. Interfacial distribution of total molar flux for a horizontal ampoule of Ar = 2, a linear wall temperature profile between Ts = 613.5 K and T_c = 593.15 K, and g_y = 1 g_0 and 0.1 g_0.

The vapor pressure[30] p_A of Hg_2Cl_2 (in the unit of Pascal) can be evaluated from the following formula as a function of temperature: in which a = 29.75, b = 11767.1.

$$p_A = e^{(a-b/T)}, \quad (5)$$

3. Results and Discussion

The purposes of this research is to investigate the effects of aspect ratio on diffusive-convection during physical vapor transport of Hg_2Cl_2 with impurity of NO, in a viewpoint of total mass flux and its interfacial distributions. Because the molecular weight of an impurity (NO) is not equal to that of the crystal component (Hg_2Cl_2) during the physical vapor transport, the effects of both thermal and solutal convection with a linear temperature profile should be considered in this study. Table 1 shows typical process parameters and physical properties for the operating conditions used in this study.

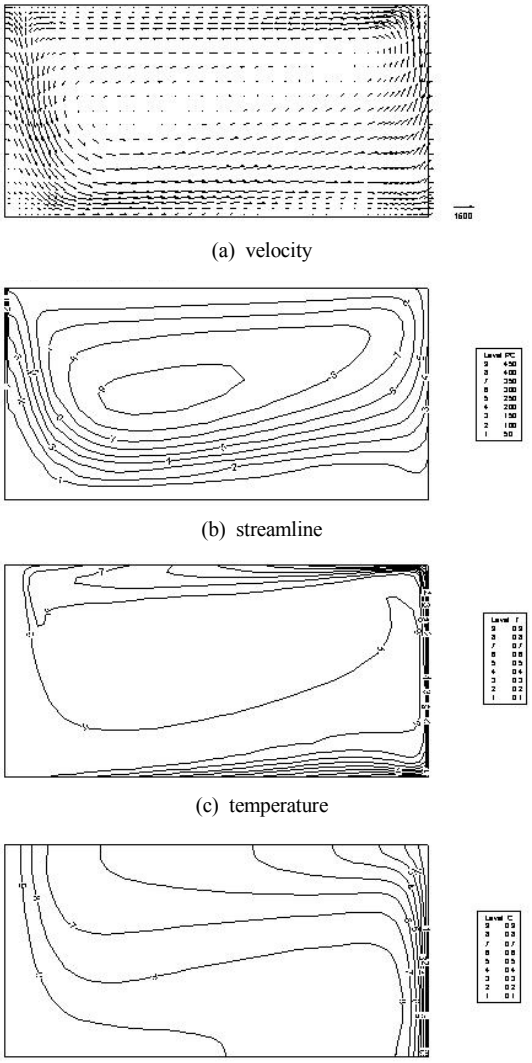

(a) velocity

(b) streamline

(c) temperature

(d) concentration

Figure 3. (a) velocity, (b) streamline, (b) temperature, (d) concentration, based on Ar = 2, △T = 20 K (613.15 K → 593.15 K), and 1 g_0. A relative velocity vector with a magnitude of 1500 has 0.0002 cm. The maximum velocity vector is 7.11 cm s^{-1}.

Figure 2 shows our numerical results for interfacial distributions of the total molar flux for two different gravitational accelerations, gy = 1 g_0 and 0.1 g_0 in the negative y-direction, where g_0 denotes the Earth's gravitational acceleration of 981 cm s^{-2}. The interfacial distributions with non-uniformities against the center of y = 2.5 cm reflect the effects of the gravitational acceleration on diffusive-convection. Process parameters of Ar (aspect ratio) = 2 (L = 10 cm, H = 5 cm), with the source temperature, Ts = 613.15 K, the crystal temperature, Tc = 593.15 K, a total operating pressure of 308 Torr are applied. Solutal convection is so one order of magnitude larger than thermal convection that thermal convection would be negligible. As shown in Figure 2, the solutal convection enhances the overall mass transport of component A (Hg_2Cl_2), and, then results in an increase in its total molar flux, but pays for the expense of uniformity in the total molar flux,

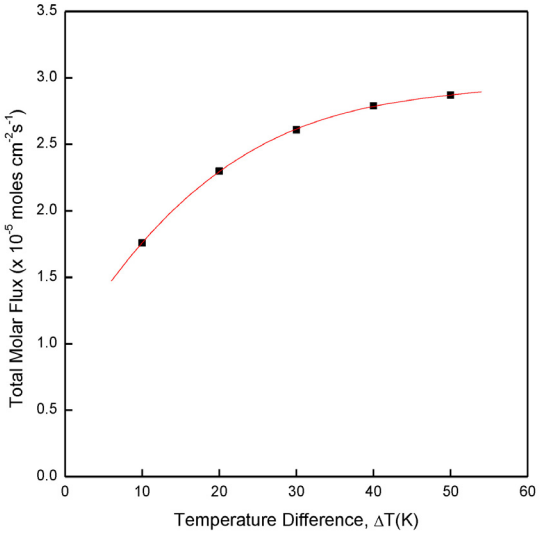

Figure 4. Effect of temperature difference between the source material and crystal region on total molar flux, between the source material and crystal region on total molar flux, for Ar = 2 (L = 5 cm), the gravity acceleration of g_y = 1 g_0.

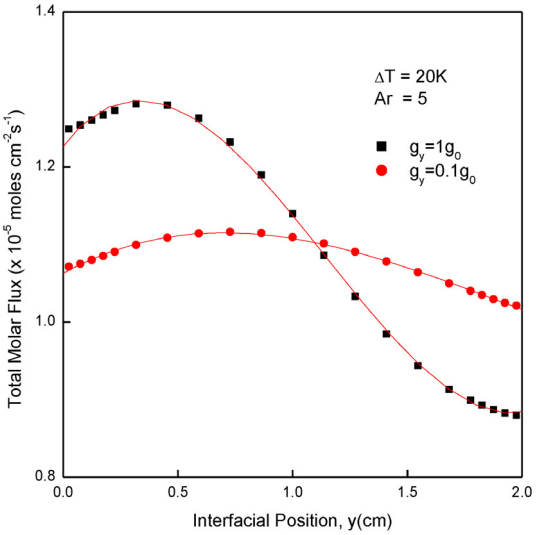

Figure 5. Interfacial distribution of total molar flux for a horizontal ampoule of Ar = 5, a linear wall temperature profile between T_s = 613.5 K and T_c = 593.15 K, and g_y = 1 g_0 and 0.1 g_0.

with the specific interfacial distribution revealing dominance of diffusive solutal convection. This result is consistent with Rosenberger's earlier results[23]. The total molar fluxes for two cases of gy = 1 g_0 and 0.1 g_0 imply the occurrence of one cell in front of the crystal region, which is found to be confirmed as shown in Figure 3, later. Their profiles are asymmetric against the center position of y = 2.5 cm. Moreover, the maximum value of the total molar flux for two cases of gy = 1 g_0 and 0.1 g_0 occurs between y = 1 cm and y = 2 cm, the maximum value of the total molar flux for the case of gy = 1 g_0 is about twice that for gy = 0.1 g_0.

An appreciation for the nature of the diffusive convective flow and the temperature, and the concentration fields can be obtained by examining plots of vector fields and streamlines and isotherms and iso-concentrations. As one sees Figure 3, the velocity vector, streamline, temperature, and concentration profiles show the essence of diffusive convection in the vapor phase, Ar = 2, △T = 20 K. One single convective cell stems from density gradients due to unequal molecular weights of A and B, associated with gravitational acceleration on earth, which indicates three dimensional diffusive convection flow structures. Similar to one's earlier findings[31], the magnitudes of velocity vector near the source region are much greater than those near the crystal region. For the process parameters under consideration, the flow structures are centered into wall boundary layers so that there should be one single cell over the entire vapor region in the enclosure. As shown in Figure 3(b), a streamline structure confirms a strong cellular convection. The temperature profile exhibits relatively strong gradients along the walls and crystal region. As shown in Figure 3(d), the mass concentrations in front of the source regions are relatively uniform, and sharply varied near the crystal regions. A relative velocity vector with 1,500 magnitudes has 0.0002 cm. The dimensional maximum magnitude of velocity vector is 7.11 cm s^{-1}.

Figure 4 shows the effect of temperature difference between the source material and crystal region on total molar flux, for Ar = 2, the gravity acceleration of gy = 1 g_0. The total molar flux increases linearly with increasing the temperature difference form 10 K up to 30 K, and is found to have a linear and direct relationship with the temperature difference, and then since 30 K, the gradient of flux against temperature has a gentle slope. In specific words, the flux is increased by a factor of 1.50 under ranges from 10 K up to 30 K, whereas it increases by a factor of 1.09 with an increase in the temperature difference from 30 K to 50 K. Therefore, it is inferred that the importance of diffusive-solutal convection is much considered compared with diffusive thermal convection.

Figure 5 shows the effect of aspect ratio on the interfacial distribution, with the same process parameters as Figure 2. In comparisons of Ar of 2 with 5, the fluxes for Ar = 2 are much greater than for Ar = 5, but the corresponding nonuniformities in interfacial distributions are also much larger, which would be due to the effect of side walls in the enclosure. Therefore, the flux and non-uniformity are dependent of the aspect ratio up to 5 under consideration. As shown in Figures 2 and 3, the diffusive convective flow structure is inherently asymmetrical at the location, y^* = 0.5. The diffusive convection vector fields, and streamlines, temperature, concentration contours illustrated in Figure 6 corresponds to Figure 5. To investigate the effect of aspect ratio on diffusive convection flow structure, the convection vector fields and streamline, temperature, concentration contours are illustrated in Figures 6(a), 6(b), 6(c) and 6(d), respectively, for Ar = 5, △T = 20 K (613.15 K → 593.15 K) and the linear temperature wall boundary condition of Eq. (2). As expected, as the aspect ratio from 2 up to 5, the convective flow is transited from asymmetrical structure to symmetric pattern, which is likely to be due to the two-dimensional wall effects.

To understand the effect of temperature difference at Ar = 5, the convection vector fields and streamline, temperature, concentration contours obtained for the △T = 50 K (613.15 K → 563.15 K) are il-

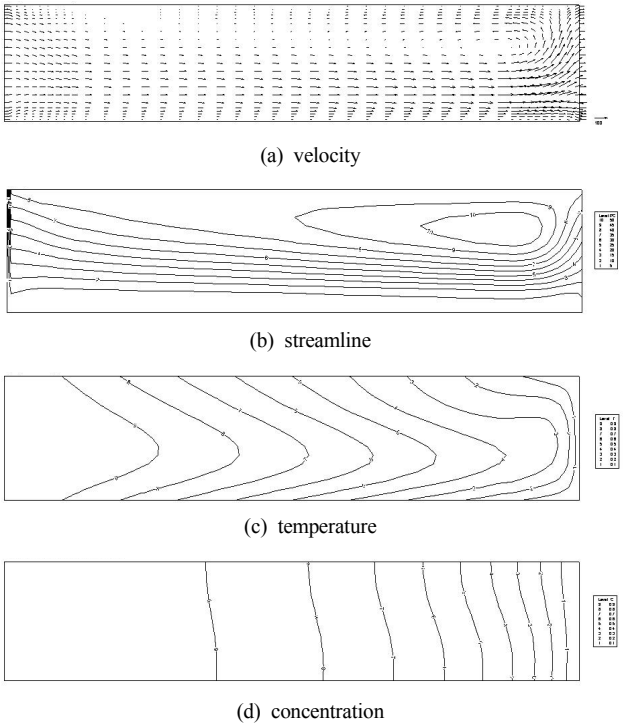

Figure 6. (a) velocity, (b) streamline, (b) temperature, (d) concentration, based on Ar = 5, △T = 20 K (613.15 K → 593.15 K), and 1 g_0. A relative velocity vector with a magnitude of 100 has 0.0035 cm. The maximum velocity vector is 0.67 cm s^{-1}.

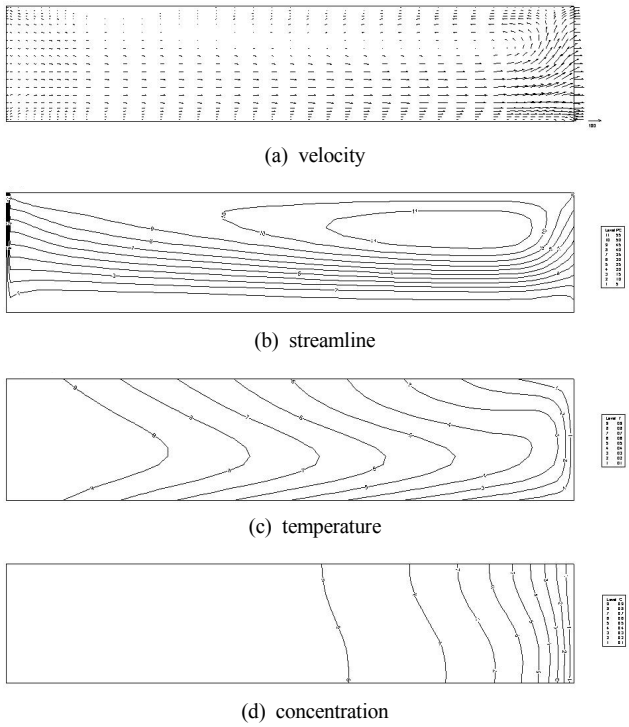

Figure 7. (a) velocity, (b) streamline, (b) temperature, (d) concentration, based on Ar = 5, △T = 50 K (613.15 K → 563.15 K), and 1 g_0. A relative velocity vector with a magnitude of 100 has 0.0035 cm. The maximum velocity vector is 1.19 cm s^{-1}.

lustrated in Figure 7. In comparison of Figure 6 with Figure 7, a single cell is dominated in the vapor phase, which indicates the convective structure is independent of temperature difference. In other words, the vector fields and streamline, temperature, concentration contours which correspond to △T = 20 K (613.15 K → 593.15 K) and △T = 50 K (613.15 K → 563.15 K) are basically similar. As plotted in Figures 3 and 6 and 7, the convective circulation pattern is counterclockwise, with flow downward at source left region and upward at the crystal right region, because of the temperature difference, i.e., driving force for physical vapor transport, the effective temperature drop driving the flow in enclosure with Ar = 5, △T = 20 K, Figure (6) is less than that for the enclosure with Ar = 5, △T = 50 K, Figure (7); as a result, the strength of the convection flow is less for the case of Figure (6) than for case of Figure (7). In specific words, the maximum velocity vectors in Figures 6 and 7 are 0.67 cm s^{-1} and 1.19 cm s^{-1}, respectively. As discussed in one's earlier paper[31], the magnitude of maximum velocity vector implies the strength of the convection flow. The temperature and concentration profiles in the vapor phase for Ar = 2, △T = 20 K, as seen in Figures 3(c) and 3(d), are quite non-uniform. This non-uniformity has a noticeable effect on the convection field so that the flow is asymmetric. Whereas the convection flow shown in Figures 6 and 7 is nearly symmetric because temperature and concentration profiles in the vapor phase for Ar = 5, as seen in Figures 3 are symmetric.

As seen in Figure 8, the equilibrium vapor pressures of composition A, $p_A(y)$ which are computed from Eq. (5) are compared with the

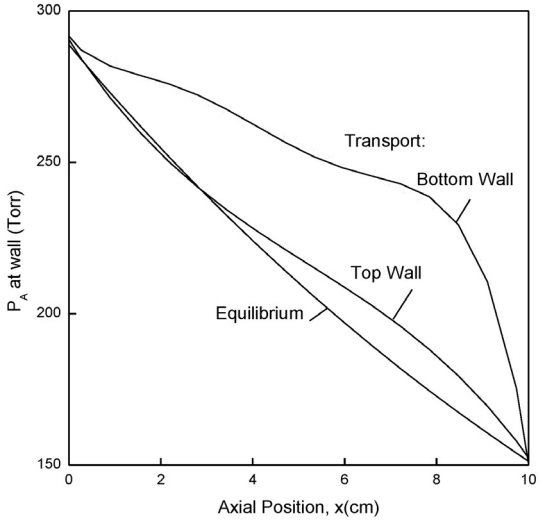

Figure 8. Axial distribution of partial pressure of component A at the walls resulting from diffusive-convective transport at 1 g_y = 1 g_0, and equilibrium vapor pressure for Ar = 2 and linear wall temperature profile between T_s = 613.15 K and T_c = 593.15 K.

$p_A(y)$'s that appear at the top and bottom walls due to diffusive-con vective transport at Ar = 2, △T = 20 K, the gravity acceleration of gy = 1 g_0. It is found that the concentrations along the bottom walls are much higher than those along the top walls. This finding reflects the counterclockwise sense of rotation of diffusive convection with one single cell. Moreover, the concentrations of component A are always

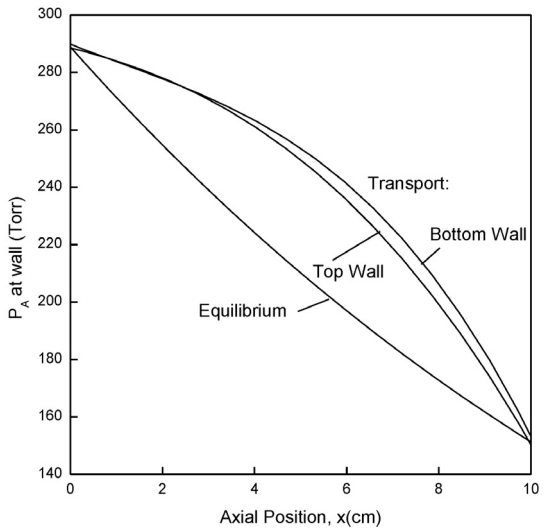

Figure 9. Axial distribution of partial pressure of component A at the walls resulting from diffusive-convective transport at 1 g_y = 1 g_0, and equilibrium vapor pressure for Ar = 5 and a linear wall temperature profile between T_s = 613.15 K and T_c = 593.15 K.

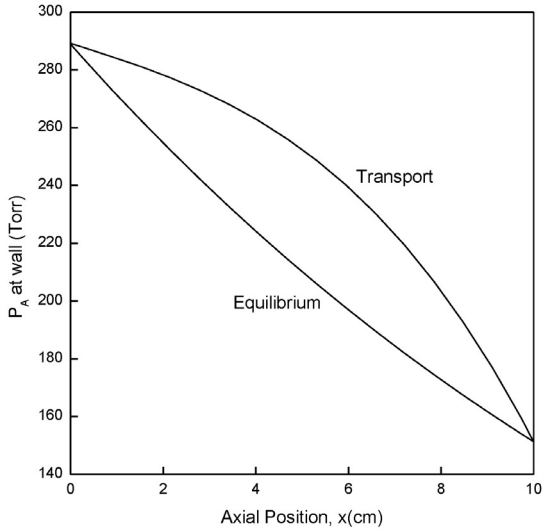

Figure 10. Axial distribution of partial pressure of component A at the walls resulting from purely diffusive transport for Ar = 5 and a linear wall temperature profile between T_s = 613.15 K and T_c = 593.15 K. The equilibrium vapor pressure profile corresponding to the wall temperature distribution is shown for comparison.

above the equilibrium vapor pressures of composition A, $p_A(y)$ so that the vapor of component A is in a supersaturated state throughout the enclosure. Because such as a supersaturated state should be avoided, a nonlinear temperature profile with maximum ("hump") is adopted in an actual crystal growth system[23]. In other words, an experimental method to prevent nucleation at enclosure walls is usually referred as a temperature "hump", which is created by imposing a wall temperature profile with a maximum between the source material and the crystal region. Therefore, it is not easy to see why a linear temperature profile is utilized in practice. Nevertheless, adoption of the linear temperature profile plays an important role as a useful tool in modeling and simulation analysis of the PVT process. Figure 9 shows axial distribution of partial pressure of component A at the same system as in Figure 8, except for Ar = 5. In comparison of Figure 8 with Figure 9, as an aspect ratio increases under conditions considered, the gaps between the bottom and the top walls get closer to each other. This result leads to the transition from the diffusive-convection to the diffusion mode due to the effect of side walls. Finally, the diffusion is predominant over the diffusion-convection so that the diffusion mode approaches to purely diffusion transport as illustrated in Figure 10. Figure 10 compares the equilibrium vapor pressure of composition A, $p_A(y)$, computed from Eq. (5) with the partial pressures of A in the enclosure walls resulting from purely diffusive transport. A system of Ar = 5, $\triangle$T = 20 K, and 10^{-3} g_0 is considered for obtaining results of purely diffusive transport.

4. Conclusions

This research investigates the effects of aspect ratio on diffusive-convection during physical vapor transport of Hg_2Cl_2-NO system. For a system with T_s = 613.51 K and T_c = 593.15 K, the gravity accelerations of 1 g_0, linear temperature profiles at walls, the total molar fluxes for Ar = 2 are much greater than Ar = 5, but the corresponding nonuniformities in interfacial distributions are also much larger due to the effects of convection. The maximum values of total molar fluxes for both cases of g_y = 1 g_0 and 0.1 g_0 appear in the neighborhood of interfacial position, y^* = 0.5. The former is greater twice than the latter. It is concluded that a factor of ten reductions in the gravitational level is not enough to suppress the convective effects on the total molar flux, but with increasing an aspect ratio from 2 to 5, a diffusive-convection mode is transited into the diffusion mode, and then the strength of diffusion is predominant over is the strength of diffusive-convection. Also, at the gravitational level of 10^{-3} g_0, the effect of convection is found to be negligible.

Acknowledgement

This research was financially supported by the 2014 Hannam University Research Fund 2014A132 (April 1, 2014 through March 31, 2015).

References

1. N. B. Singh, M. Gottlieb, G. B. Brandt, A. M. Stewart, R. Mazelsky, and M. E. Glicksman, Growth and characterization of mercurous halide crystals: mercurous bromide system, *J. Crystal Growth*, **137**, 155-160 (1994).
2. N. B. Singh, R. H. Hopkins, R. Mazelsky, and J. J. Conroy, Purification and growth of mercurous chloride single crystals, *J. Crystal Growth*, **75**, 173-180 (1986).
3. S. J. Yosim and S. W. Mayer, The mercury-mercuric chloride system, *J. Phys. Chem.*, **64**, 909-911 (1960).
4. T. Yamaguchi, K. Ohtomo, S. Sato, N. Ohtani, M. Katsuno, T.

Fujimoto, S. Sato, H. Tsuge, and T. Yano, Surface morphology and step instability on the (0001)C facet of physical vapor transport-grown 4H-SiC single crystal boules, *J. Crystal Growth*, **431**, 24-31 (2015).
5. C. Ohshige, T. Takahashi, N. Ohtani, M. Katsuno, T. Fujimoto, S. Sato, H. Tsuge, T. Yano, H. Matsuhata, and M. Kitabatake, Defect formation during the initial stage of physical vapor transport growth of 4H-SiC in the (1120) direction, *J. Crystal Growth*, **408**, 1-6 (2014).
6. J. G. Kim, J. H. Jeong, Y. Kim, Y. Makarov, and D. J. Choi, Evaluation of the change in properties caused by axial and radial Temperature gradients in silicon carbide crystal growth using the physical vapor transport method, *Acta. Materialia*, **77**, 54-59 (2014).
7. Y. Shi, J. Yang, H. Liu, P. Dai, B. Liu, Z. Jin, and G. Qiao, Fabrication and mechanism of 6H-type silicon carbide whiskers by physical vapor transport technique, *J. Crystal Growth*, **349**, 68-74 (2012).
8. M. A. Fanton, Q. Li, A. Y. Polyakov, and M. Skowronski, Electrical properties and deep levels spectra of bulk SiC crystals grown by hybrid physical-chemical vapor transport method, *J. Crystal Growth*, **300**, 314-318 (2007).
9. K. Semmelroth, M. Krieger, G. Pensl, H. Nagasawa, R. Pusche, M. Hundhausen, L. Ley, M. Nerding, and H. P. Strunk, Growth of cubic SiC single crystals by the physical vapor transport technique, *J. Crystal Growth*, **308**, 241-246 (2007).
10. E. R. Letts, J. S. Speck, and S. Nakamura, Effect of indium on the physical vapor transport growth of AIN, *J. Crystal Growth*, **311**, 1060-1064 (2009).
11. J. T. Mullins, F. Dierre, and B. K. Tanner, X-ray diffraction imaging of ZnTe Crystals grown by the multi-tube physical vapour transport technique, *J. Crystal Growth*, **431**, 61-68 (2015).
12. L. Hongtao, S. Wenbin, M. Jiahua, and Z. Feng, Purification of $Cd_{0.9}Zn_{0.1}Te$ by physical vapor transport method, *Mater. Lett.*, **59**, 3837-3840 (2005).
13. H. Cai, W. Wang, P. Liu, G. Wang, A. Liu, Z. He, Z. Cheng, S. Zhang, and M. Xia, Enhanced synthesis of Sn nanowires with aid of Se atom via physical vapor transport, *J. Crystal Growth*, **420**, 42-46 (2015).
14. S. Jo, S. Suzuki, and M. Yoshimura, Effect of solid-state polymerization on crystal morphology of a type of polydiacetylene single crystal obtained by physical vapor transport technique," *Thin Solid Films*, **554**, 154-157 (2014).
15. S. Collins, S. Vatavu, V. Evani, M. Khan, S. Bakhshi, V. Palekis, C. Rotaru, and C. Ferekides, Radiative recombination mechanisms in CdTe thin films deposited by elemental vapor transport, *Thin Solid Films*, **582**, 139-145 (2015).
16. S. Y. Hung, R. L. Kao, K. Y. Lin, C. C. Yang, K. S. Lin, Y. C. Chao, J. S. Wang, J. L. Shen, and K. C. Chiu, Characterization of facial and meridional Alq_3 thin films fabricated from physical vapor transport at high substrate temperatures, *Mater. Chem. Phys.*, **154**, 100-106 (2015).
17. A. Choubey, P. Veeramani, A. T. G. Pym, J. T. Mullins, P. J. Sellin, A. W. Brinkman, I. Radley, A. Basu, and B. K. Tanner, Growth by the Multi-tube Physical Vapour Transport Method and Characterization of Bulk (Cd, Zn)Te, *J. Crystal Growth*, **352**, 120-123 (2012).
18. Y. Shi, J. F. Yang, H. Liu, P. Dai, B. Liu, Z. Jin, G. Qiao, and H. Li, Fabrication and Mechanism of 6H-type Silicon Carbide Whiskers by Physical Vapor Transport Technique, *J. Crystal Growth*, **349**, 68-74 (2012).
19. N. Zotov, S. Baumann, W. A. Meulenberg, and R. Vaßen, La-Sr-Fe-Co Oxygen Transport Membranes on Metal Supports Deposited by Low Pressure Plasma Spraying-Physical Vapour Deposition, *J. Membrane Sci.*, **442**, 119-123 (2013).
20. M. A. Fanton, Q. Li, A. Y. Polyakov, M. Skowronski, R. Cavalero, and R. Ray, Effects of Hydrogen on the Properties of SiC Crystals Grown by Physical Vapor Transport: Thermodynamic Considerations and Experimental Results, *J. Crystal Growth*, **287**, 339-343 (2006).
21. C. H. Su, M. A. George, W. Palosz, S. Feth, and S. L. Lehoczky, Contactless Growth of ZnSe Single Crystals by Physical Vapor Transport, *J. Crystal Growth*, **213**, 267-275 (2000).
22. C. Paorici, C. Razzetti, M. Zha, L. Zanotti, L. Carotenuto, and M. Ceglia, Physical Vapour Transport of Urotropine: One-Dimensional Model, *Mater. Chem. and Phys.*, **66**, 132-137 (2000).
23. A. Nadarajah, F. Rosenberger, and J. Alexander, Effects of buoyancy-driven flow and thermal boundary conditions on physical vapor transport, *J. Crystal Growth*, **118**, 49-59 (1992).
24. F. Rosenberger, J. Ouazzani, I. Viohl, and N. Buchan, Physical vapor transport revised, *J. Crystal Growth*, **171**, 270-287 (1997).
25. P. A. Tebbe, S. K. Loyalka, and W. M. B. Duval, Finite element modeling of asymmetric and transient flowfields during physical vapor transport, *Finite Elem. Anal. Des.*, **40**, 1499-1519 (2004).
26. M. Alsaady, R. Fu, B. Li, R. Boukhanouf, and Y. Yan, Thermo-physical properties and thermo-magnetic convection of ferrofluid, *Appl. Therm. Eng.*, **88**, 14-21 (2015).
27. T. Qin, Z. Tukovic, and R. O. Grigoriev, Buoyancy-thermocapillary convection of volatile fluids under their vapors, *Int. J. Heat Mass Transfer*, **80**, 38-49 (2015).
28. F. Rosenberger and G. Müller, Interfacial transport in crystal growth, a parameter comparison of convective effects, *J. Crystal Growth*, **65**, 91-104 (1983).
29. S. V. Patankar, *Numerical Heat Transfer and Fluid Flow*, Hemisphere Publishing Corp., Washington D. C., (1980).
30. B. S. Jhaveri and F. Rosenberger, Expansive Convection in Vapor Transport across Horizontal Enclosures, *J. Crystal Growth*, **57**, 57-64 (1982).
31. G. T. Kim and M. H. Kwon, Effects of solutally dominant convection on physical vapor transport for a mixture of Hg_2Br_2 and Br_2 under microgravity environments, *Korean Chem. Eng. Res.*, **52**, 75-80 (2014).